Climate Dynamics (2022) 59:2517–2529
https://doi.org/10.1007/s00382-022-06312-2

Role of ocean dynamics in equatorial Pacific decadal variability

Yu Zhang[1,2] · Shi-Yun Yu[1,3] · Shang-Ping Xie[4] · Dillon J. Amaya[5] · Qihua Peng[4] · Yu Kosaka[6] · Xiaopei Lin[1,2] · Jun-Chao Yang[1,2] · Sarah M. Larson[7] · Arthur J. Miller[4] · Lei Fan[1,3]

Received: 10 November 2021 / Accepted: 23 April 2022 / Published online: 27 May 2022

Abstract

The tropical Pacific exhibits decadal El Niño-Southern Oscillation (ENSO)-like variability, characterized by meridionally broad sea surface temperature anomalies in the eastern Pacific. In this study, we focus on the variability in the equatorial Pacific band (5°S–5°N), termed equatorial Pacific decadal variability (EPDV). While it is known that ocean dynamics plays an essential role in EPDV, the simulations by air-sea thermodynamically coupled slab ocean models (SOM) obscure the nature of the role of ocean dynamics. To confront this issue, we use a mechanically decoupled simulation, which isolates the effects of thermodynamic coupling processes and mean ocean circulation on EPDV. Thus, by comparing the simulation to a SOM, we investigate the role of mean ocean circulation and show that it plays a role in damping EPDV, primarily through mean equatorial Pacific upwelling. By comparing the simulation to a fully coupled dynamic ocean model (DOM), we examine the role of anomalous wind-driven ocean circulation and demonstrate that it plays a role in amplifying EPDV. Further, this amplification strength overwhelms the upwelling damping effect, resulting in the anomalous wind-driven ocean circulation forcing EPDV. Finally, we examine the origin of EPDV in the DOM and show that it originates from a zonal dipole mode in the tropical Pacific, which is strongly associated with decadal modulation of ENSO amplitude. Taking EPDV as an example, our study advances the understanding of the two distinct dynamical systems (SOM and DOM), benefiting the physical interpretation of other climate variabilities.

Keywords Equatorial Pacific · Decadal variability · Ocean dynamics · Coupled model experiment

✉ Yu Zhang
zhangyu@ouc.edu.cn

✉ Xiaopei Lin
linxiaop@ouc.edu.cn

1 Frontier Science Center for Deep Ocean Multispheres and Earth System (FDOMES) and Physical Oceanography Laboratory, Ocean University of China, Qingdao, China

2 Qingdao National Laboratory for Marine Science and Technology, Qingdao, China

3 College of Oceanic and Atmospheric Sciences, Ocean University of China, Qingdao, China

4 Scripps Institution of Oceanography, University of California San Diego, La Jolla, San Diego, CA, USA

5 Physical Science Laboratory, Earth System Research Laboratory, National Oceanic and Atmospheric Administration, Boulder, CO, USA

6 Research Center for Advanced Science and Technology, The University of Tokyo, Tokyo, Japan

7 Department of Marine, Earth and Atmospheric Sciences, North Carolina State University, Raleigh, NC, USA

1 Introduction

In the tropical Pacific (~ 30°S–30°N), El Niño-Southern Oscillation (ENSO) is the dominant mode of ocean–atmosphere coupled variability on interannual timescales, with strong amplitude in the equatorial Pacific (5°S–5°N) sea surface temperature anomalies (SSTAs; Timmermann et al. 2018). Additionally, the tropical Pacific also exhibits pronounced ENSO-like variability on decadal timescales, but with meridionally broader SSTAs in the eastern Pacific (Zhang et al. 1997), referred to as tropical Pacific decadal variability (TPDV; Power et al. 2021). TPDV in the north and south of extra-equatorial Pacific manifest as decadal variability of the North and South Pacific Meridional Mode (NPMM and SPMM), respectively (Liu et al. 2019; Zhang et al. 2021). While decadal variability of both NPMM and SPMM was suggested to be generated mainly by North and South Pacific atmospheric forcing, respectively (Zhang et al. 2021), the mechanism of TPDV in the equatorial Pacific, the variability referred to as equatorial Pacific decadal

variability (EPDV) in this study, is under debate (Okumura 2013; Zhang et al. 2014a; Power et al. 2021). Therefore, we focus on EPDV in the rest of this study.

A number of studies suggested that EPDV is generated by ocean–atmosphere dynamic coupling, with interactive ocean dynamical processes involved (Power et al. 2021). One school of notions argued that EPDV is the residual of dynamic coupled ENSO variability, known as the null hypothesis (Vimont 2005; Power and Colman 2006). Additionally, EPDV was also suggested to be interacted with ENSO variability (Chang et al. 2007; Choi et al. 2009, 2012, 2013; Di Lorenzo et al. 2015). Specifically, EPDV can be generated by the nonlinearities of ENSO in amplitude and spatial pattern that rectify into the tropical Pacific mean state (Timmermann et al. 2003; Watanabe and Wittenberg 2012; Ogata et al. 2013; Sun et al. 2014; Hua et al. 2015; Kim and Kug 2020). The mean state changes, in turn, can also change ENSO characteristics (Cobb et al. 2003; An 2009; Sun and Yu 2009; Li et al. 2011). Therefore, EPDV and ENSO variability form a two-way interactive feedback (Choi et al. 2009; Sun and Yu 2009).

In contrast, other schools suggested that EPDV originates from decadal-scale dynamic coupling processes in the tropical Pacific. For example, oceanic Rossby waves excited by the extra-equatorial Pacific wind stress curl anomalies propagate westward, reaching at the western boundary and turning to coastally and then equatorially trapped Kelvin waves, which propagate eastward and affect the depth of the equatorial thermocline, thereby impacting SSTAs (Capotondi and Alexander 2001; Meehl and Hu 2006). Additionally, changes in the strength of the subtropical-tropical cells affected by wind stress anomalies will alter the strength of equatorial Pacific upwelling, thus EPDV (McPhaden and Zhang 2002; Capotondi et al. 2005; Graffino et al. 2019). Apart from the abovementioned mechanisms of EPDV that originate from the tropical Pacific, some studies proposed that EPDV can be generated from extra-tropical Pacific variability (Barnett et al. 1999; Pierce et al. 2000; Luo and Yamagata 2001; Dommenget and Latif 2008; Liguori and Di Lorenzo 2019; Sun and Okumura 2019; Zhao and Di Lorenzo 2020; Yang et al. 2021). For instance, some of the studies suggested that EPDV mostly originates from the South Pacific (Luo and Yamagata 2001; Tatebe et al. 2013; Liguori and Di Lorenzo 2019; Sun and Okumura 2019) because of the northward displaced Intertropical Convergence Zone (ITCZ), which facilitates ocean–atmosphere thermodynamic and dynamic coupling processes from the South Pacific to affect EPDV (Zhang et al. 2014b; Sun and Okumura 2019). All the EPDV mechanisms mentioned above can be simulated by the atmosphere coupled with dynamic ocean models (DOM). The simulated EPDV with extra-equatorial Pacific SSTAs exhibit symmetric pattern about the equator, similar to that seen in observations (Power et al. 2021).

EPDV, however, can also be simulated by the atmosphere coupled with slab ocean models (SOM), in which the ocean is motionless and thus only air-sea thermodynamic coupling processes affect SSTAs (Clement et al. 2011; Okumura 2013; Zhang et al. 2014a). EPDV in SOM is suggested to be originated from the subtropical southeastern Pacific, where the SSTAs are stochastically forced by South Pacific atmospheric variability (Okumura 2013; Zhang et al. 2014a). The initiated SSTAs then propagate northwest onto the equator via the wind-evaporation-SST (WES) feedback (Xie and Philander 1994). The simulated EPDV and associated extra-equatorial Pacific SSTAs exhibit asymmetric structure about the equator—much stronger in the southeastern Pacific—a pattern distinct from that in observations and DOM (Okumura 2013; Zhang et al. 2014a).

The distinct pattern suggests that ocean dynamics is essential in shaping the EPDV-associated SSTA pattern, which has been pointed out in previous studies (Clement et al. 2011; Power et al. 2021). It remains unclear, however, what role ocean dynamics plays in EPDV, giving rise to the simulations by the two distinct complexities of coupled model experiments (i.e., SOM and DOM). This ambiguity may arise from the gap in the dynamical framework between SOM and DOM (Larson et al. 2018a). In DOM, both mean and anomalous ocean circulation driven respectively by mean and anomalous wind stress impact SSTAs. Therefore, isolating their individual role in EPDV may help to unravel the ambiguity.

To do so, in this study we used a mechanically decoupled experiment, named Clim-τ, in which ocean–atmosphere dynamic coupling in the tropical Pacific was disengaged by prescribing climatological wind stress (Zhang et al. 2021). By this design, the effect of anomalous ocean circulation driven by the anomalous wind stress on SSTAs was removed. Consequently, the Clim-τ partly fills the dynamical gap between SOM and DOM. By comparing SOM to the Clim-τ, we explored the role of mean ocean circulation in EPDV; by comparing the Clim-τ to DOM, we investigated the role of anomalous wind stress-driven ocean circulation in EPDV. We found that the former plays a role in damping EPDV, mainly through mean equatorial Pacific upwelling, while the latter plays a role in amplifying the EPDV. Further, by performing mixed-layer heat budget analysis, we demonstrated that anomalous ocean circulation is the driver of EPDV. Our study advances the understanding on the similarity in EPDV between the two distinct dynamical systems (SOM and DOM) by virtue of the Clim-τ, with potential implications for understanding the role of ocean dynamics in other climate variabilities and ocean basins.

The rest of the paper is organized as follows. Section 2 introduces the model configurations of SOM, the Clim-τ, and DOM, as well as the definition of EPDV and a mixed-layer heat budget analysis. Section 3 presents the results of

how mean ocean circulation and anomalous wind-driven ocean circulation play the roles in damping and amplifying EPDV, respectively. Subsequently, the heat budget analysis will be used to identify the key oceanic feedback processes driving EPDV. The origin of EPDV will be explored based on DOM in Sect. 4. Section 5 is the summary with discussions.

2 Data and methods

2.1 A hierarchy of coupled model experiments

The Clim-τ and DOM experiments were based upon the Geophysical Fluid Dynamic Laboratory coupled model version 2.1 (CM2.1; Delworth et al. 2006). The model consists of the atmospheric model version 2.1 (AM2.1) with a horizontal resolution of 2.5° longitude × 2° latitude and the Modular Ocean Model version 4.1 with a horizontal resolution of 1° longitude × 1° latitude poleward of 30°. The latitudinal resolution equatorward of 30° in the ocean model gets gradually finer to 1/3° at the equator. All model outputs were monthly mean data.

For SOM, we used a motionless, constant-depth slab ocean coupled with AM2.1 (Stouffer et al. 2006), which only simulates air-sea thermodynamic coupling processes affecting SSTAs. The output of the SOM was directly available from the NOAA GFDL database (see data availability). The length of the SOM experiment was 100 years; mixed layer depth (MLD) was fixed at 50 m globally. Although the simulation length of the SOM may be short, the SOM was still sufficient to investigate EPDV, as EPDV in the SOM is the most dominant decadal variability in the equatorial Pacific SSTAs (89.5% explained variance) and statistically significant at the 95% confidence level (Fig. 2a).

For the Clim-τ, we prescribed wind stresses over the tropical Pacific with daily climatological values obtained from a 1000 year DOM (described below). The prescribed region is 15°S–15°N with 10° buffer zone north and south where the simulated and prescribed wind stresses are blended, with the weight linearly tapering off (see Fig. 1 in Zhang et al. 2021). In order to suppress tiny day-to-day fluctuations that remain in the 1000 year climatology, the prescribed wind stress had been weakly smoothed temporally by removing the annual harmonics higher than 18 (corresponding to a frequency of about (20 days)$^{-1}$). This Clim-τ experiment is the same as mechanically decoupling the DOM (Larson and Kirtman 2015; Larson et al. 2018a, b), except that only the tropical Pacific is mechanically decoupled. One should note that in the tropical Pacific, air-sea thermodynamic coupling processes are still retained, since wind speed and thereby turbulent heat flux can vary. In addition, although the anomalous wind stress-driven ocean circulation is removed, the anomalous ocean circulation driven by buoyancy (thermodynamic and freshwater flux) forcing still exists. Furthermore, other ocean processes, such as mixing, diffusion, and entrainment,

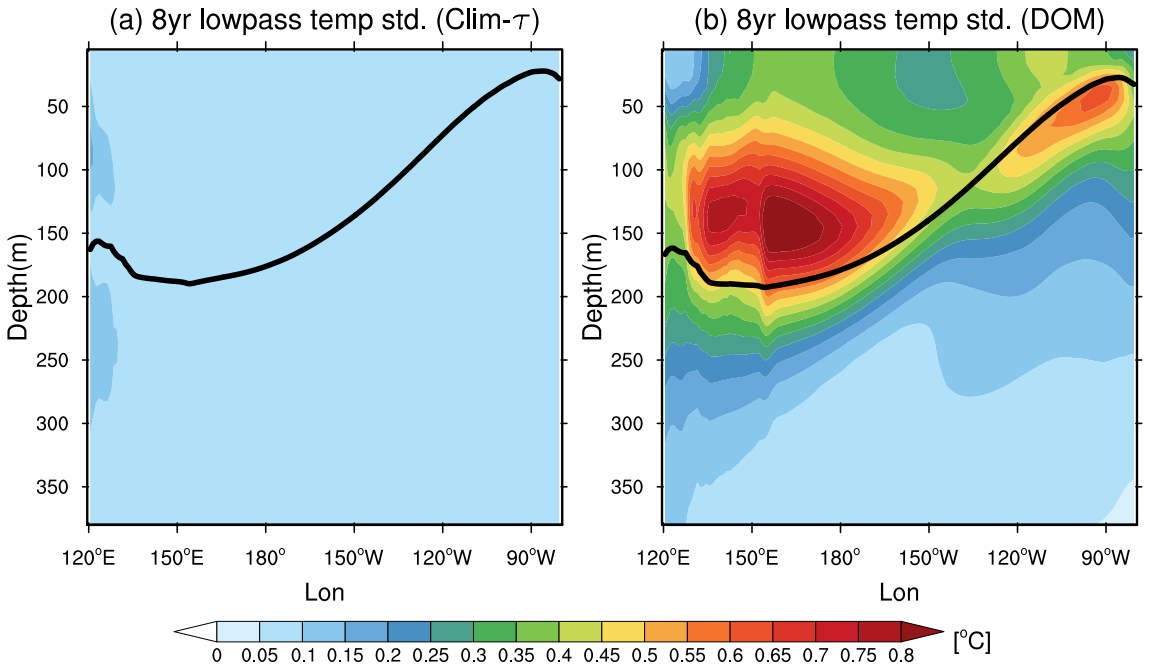

Fig. 1 Standard deviations (shading; °C) of 8 year low-pass filtered monthly ocean temperature anomalies in the equatorial Pacific (5°S–5°N meridionally averaged) in the (**a**) Clim-τ and (**b**) DOM. Black contours denote climatological 20 °C isotherm in the Clim-τ and DOM, respectively

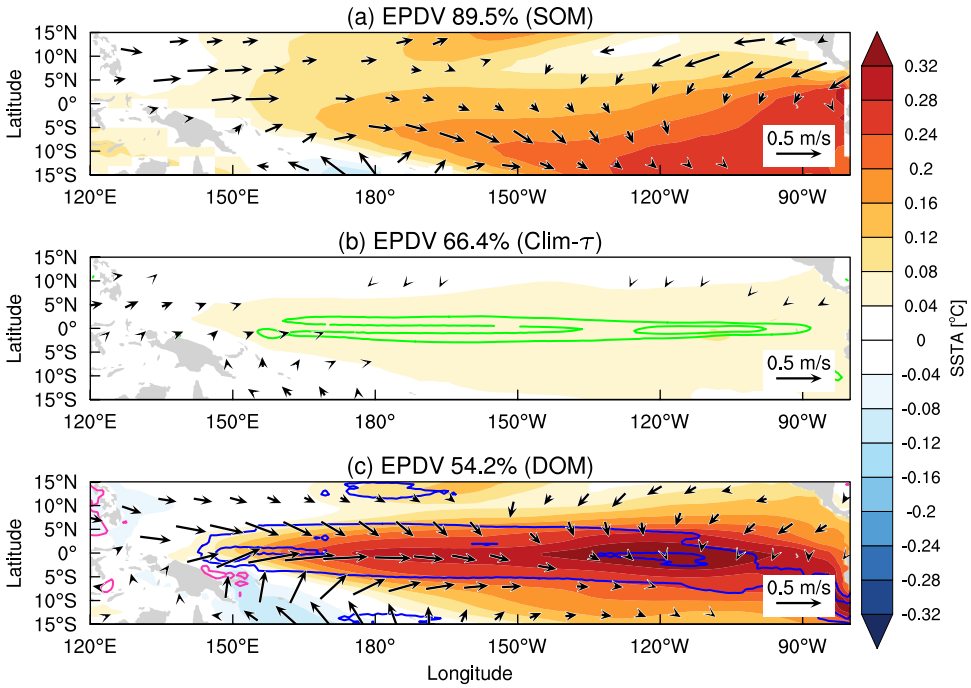

Fig. 2 EPDV patterns in the three experiments. Regression maps of 8 year low-pass filtered monthly SST (shading; °C), surface wind (vectors; m s^{-1}), and surface net heat flux anomalies (contour interval: 1 W $m.^{-2}$; purple is positive and blue is negative; downward positive) against normalized PC time series of EPDV. **a** SOM, **b** Clim-τ (mean upwelling velocity is green contour), and **c** DOM. The regressions significant at the 95% confidence level based on a two-tailed Student's *t* test are shown only, except for the regressed net heat flux, which is shown as a whole for clarity. In **a** and **b**, the surface net heat flux anomalies are too weak and thus no contour appears. The explained variance of EPDV for each experiment is labeled in the title

were also simulated. Outside the tropical Pacific, the ocean and atmosphere are fully coupled and free to evolve. The Clim-τ experiment was branched off at year 501 from the DOM simulation (thus the initial condition was already in a near-equilibrium state) and integrated for 310 years, and only the last 300 years were analyzed, since the truncation of the first 10 years ensures the ENSO signal to dissipate. It is worth noting that MLD in the Clim-τ varies in both space and time, distinct from the 50-m constant MLD in the SOM. The Clim-τ experiment was used for investigating decadal variability of NPMM and SPMM without equatorial Pacific influence in Zhang et al. (2021). Moreover, the simulation length of the experiment can also be sufficient to statistically (at the 95% confidence level) examine EPDV in this study (Fig. 2b). More details on the Clim-τ configuration can be referred to Zhang et al. (2021).

Finally, we integrated a 1000 year DOM, which includes both buoyancy and dynamic coupling globally. For the dynamic coupling, DOM contains the effects of both mean and anomalous wind-driven ocean circulations and their impact on SSTAs. It also contains other ocean processes, such as mixing, diffusion, and entrainment. The long 1000 year DOM simulation is sufficient to statistically (at the 95% confidence level) investigate EPDV (Fig. 2c).

2.2 EPDV definition

We used empirical orthogonal function (EOF) analysis to define EPDV. We defined EPDV as the first EOF mode (EOF1) of 8 year low-pass filtered monthly SSTAs in the equatorial Pacific (5°S–5°N). The EOF analysis based on 10 year or 20 year low-pass filter does not change the main conclusions of this study, although performing the 20 year low-pass filtered EOF analysis will derive EPDV as the second EOF mode in the DOM, because the variability of the EOF1 in the DOM, characterized by a zonal dipole pattern and suggested to be related to ENSO amplitude decadal modulation (Rodgers et al. 2004; Yeh and Kirtman 2004; see Fig. 5a), is stronger than EPDV on longer than 20 year timescales.

2.3 A mixed-layer heat budget analysis

To investigate the role of anomalous ocean circulation in the temporal evolution of EPDV, we conducted a mixed-layer heat budget analysis in the DOM. The heat budget equation is formulated as:

$$T_t' = \frac{Q'}{\rho c_p H} - \overline{w}\frac{T_s'}{2H} - u'\overline{T}_x - u'T_x' - v'\overline{T}_y - v'T_y' - w'\frac{\overline{T}_s - \overline{T}_e}{2H} + \overline{w}\frac{T_e'}{2H} - w'\frac{T_s' - T_e'}{2H} + R, \quad (1)$$

where T is mixed-layer temperature; Q is net surface heat flux; ρ is the density of seawater, 1022.4 kg m^{-3}; c_p is the specific heat of seawater, 3940 J kg^{-1} $°C^{-1}$; u, v, and w are zonal, meridional, and vertical velocity, respectively; H is MLD, defined as monthly climatology of the depth at which the ocean temperature is lower than the 5 m value by 0.5 °C (Kim et al. 2007); T_s is SST and T_e is the temperature at

thermocline depth, which is defined as the double of MLD. Overbar denotes monthly climatology, and prime denotes monthly anomaly departure from the corresponding monthly climatology. The subscripts t, x, and y denote the partial derivative of variables with respect to time, zonal, and meridional dimension, respectively.

The term on the left-hand side (LHS) of Eq. (1) represents the tendency of mixed-layer temperature anomaly. The first term on the right-hand side (RHS) represents the forcing of net surface heat flux anomaly. The second term represents upwelling damping, the dominant process in the role of mean ocean circulation in EPDV inferred from the Clim-τ (see Sect. 3); advections of mixed-layer temperature anomalies by mean zonal and meridional circulations are unimportant inferred from the Clim-τ and thus grouped to the residual term R. This term also includes oceanic mixing, diffusion, entrainment, sub-monthly ocean dynamical processes, and so forth. The third to the last second term on the RHS represent the effects of anomalous ocean circulation on mixed-layer temperatures. Note that although the term $\overline{w}\frac{T_e}{2H}$ is related to the effect of mean vertical motion, it represents the effect of anomalous wind-driven ocean circulation as the variability of subsurface temperature anomaly T_e' on decadal timescales (> 8 years) is primarily induced by anomalous wind-driven ocean dynamics, which can be clearly seen from the large standard deviation of subsurface temperature decadal variability in the DOM compared to that in the Clim-τ (Fig. 1). In addition, separating the term $\overline{w}\frac{T_e}{2H}$ from total mean vertical advection was typically used in most of ENSO studies, representing thermocline feedback (e.g., Jin et al. 2006; Santoso et al. 2017).

For the heat budget terms of Eq. (1) associated with zonal and meridional current, we computed them in each month and at each grid point and then averaged over MLD and over the Niño-4 (160°E–150°W, 5°S–5°N) and Niño-3 (150°W–90°W, 5°S–5°N) regions (DiNezio et al. 2012; Capotondi 2013), respectively. For the heat budget terms of Eq. (1) associated with vertical velocity, we took the value of vertical velocity at MLD, computed the vertical advection terms in each month, at each grid point, and then averaged over the Niño-4 and Niño-3 regions, respectively. Finally, we performed lead-lag regressions of each 8 year low-pass filtered heat budget term against normalized EPDV principal component (PC) in the DOM (Figs. 7 and 8).

3 Role of ocean dynamics in EPDV

We explore the roles of mean ocean circulation and anomalous wind-driven ocean circulation in EPDV via a step-by-step comparison among the SOM, Clim-τ, and DOM. Figure 2 shows the regression maps of 8 year low-pass filtered monthly SST, surface wind, and surface net heat flux anomalies against the corresponding normalized EPDV PC in each experiment. The results show that in the SOM, EPDV exhibits strong SSTAs in the southeast Pacific and moderate SSTAs in the northeast Pacific (Fig. 2a). Further analysis suggests that this equatorial asymmetry in the SSTAs mainly results from the distinct intensification of shortwave radiative flux anomaly between the southeast and northeast Pacific (Fig. 3); in contrast, the asymmetry is not attributed to the different strength of the WES feedback, which mainly arises from the distinct magnitude of climatological latent heat flux (Fig. 3b). The conclusion of the analysis is not affected even if the domains of the SSTAs are slightly changed (not shown). The SSTAs strongly correlate with surface wind anomalies, which are characterized by westerly anomalies over the western and central tropical Pacific and cross-equatorial northerly anomalies flowing towards the southeast Pacific (Fig. 2a). The EPDV pattern in the SOM resembles that simulated in other SOMs (Okumura 2013; Zhang et al. 2014a). Previous studies pointed out that EPDV in SOMs originates from the southeast Pacific SSTAs that propagate onto the equator primarily through the WES feedback (Zhang et al. 2014a). Note that on decadal timescales, changes in the upper-ocean temperature are in a quasi-equilibrium (i.e., all the processes that force SSTAs are quasi-balanced with all the damping processes). As a result, net surface heat flux anomaly associated with the EPDV in the SOM is rather weak (no contours in Fig. 2a) because it is the only driver for SSTAs.

Surprisingly, in the Clim-τ (Fig. 2b), EPDV-related SSTAs are markedly damped. Due to the same thermodynamic coupling processes as in the SOM, this damping is attributed to the effects of mean wind-driven ocean circulation, buoyancy-driven anomalous ocean circulation, and other ocean processes (e.g., mixing, diffusion, entrainment). To investigate the effect of mean wind-driven ocean circulation on EPDV, we estimate the damping/intensification rate of each dimension of mean ocean circulation acting on the EPDV-associated SSTAs. The damping/intensification rate is computed by the EPDV-associated SSTAs (SSTA pattern of Fig. 2a) gradient advected by annual-mean ocean circulation (obtained from the Clim-τ) divided by the EPDV-associated SSTAs. The result shows that mean ocean circulation plays a role in damping EPDV (within 5°S–5°N; Fig. 4d), dominantly attributed to equatorial Pacific mean upwelling (green contours in Figs. 2b and 4). The estimated damping rate of the mean upwelling on the equator is about 0.2–0.6 mon^{-1} (Fig. 4c), indicating its critical role in damping EPDV. Off the equator, the total effect of 3D mean ocean circulation on the EPDV-related SSTAs exhibits both damping and intensification effects (Fig. 4d). The intensification effect, therefore, should be overwhelmed by the stronger damping effect from buoyance-driven ocean circulation and

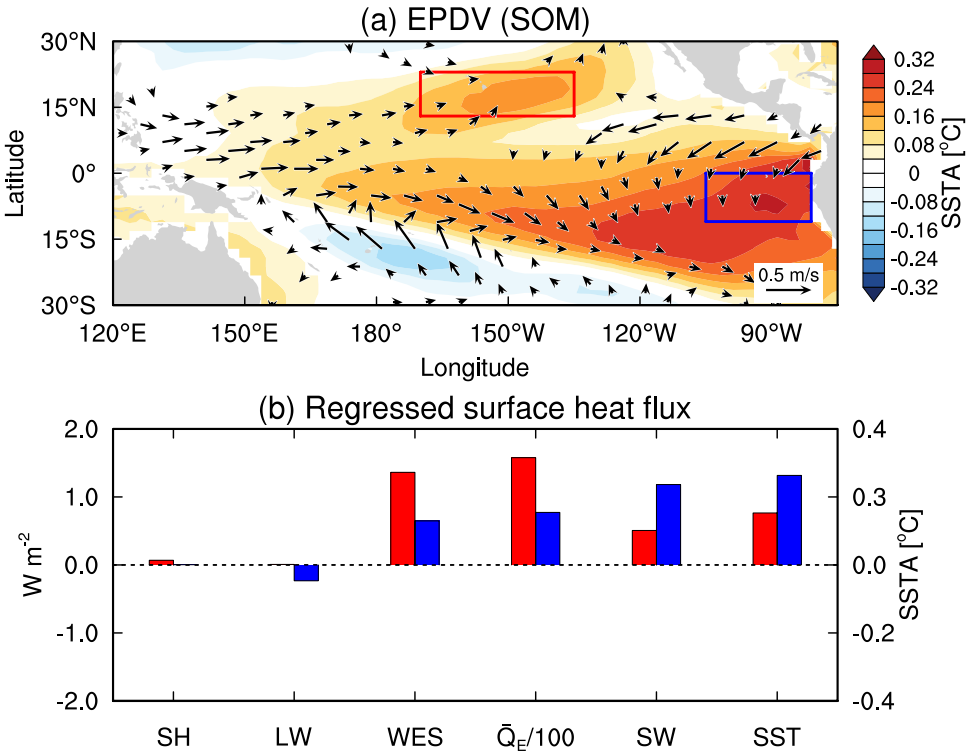

Fig. 3 Equatorial asymmetry of the EPDV-related SSTAs in the SOM. **a** Regressed tropical Pacific 8 year low-pass filtered monthly SSTAs (°C) and surface wind anomalies (m s^{-1}) against normalized EPDV PC. Red and blue boxes represent the locations of maximum SSTAs off the equatorial Pacific, respectively. **b** Regressed 8 year low-pass filtered surface heat flux anomaly (*SH* sensible heat; *LW* longwave; *SW* shortwave; *WES* WES feedback; W $m.^{-2}$) against normalized 8 year low-pass filtered SSTAs averaged in the red (red bars) and blue (blue bars) boxes. The WES feedback is calculated by $-\overline{Q_E}W'/\overline{W}$, where Q_E is latent heat flux and W is wind speed (overbar denotes climatology and prime denotes anomaly departure from the climatology). $\overline{Q_E}$ averaged over the two boxes is plotted (scaled by 1/100). The magnitudes of the 8 year low-pass filtered SSTAs averaged over the two boxes are plotted for comparison

other ocean processes (e.g., mixing, diffusion, entrainment), resulting in the mostly damped EPDV-related SSTAs off the equator in the Clim-τ (Fig. 2b).

The dominant damping effect by equatorial Pacific mean upwelling, in fact, acts not only on decadal but also on inter-decadal to multi-decadal timescales. To illustrate this point, we perform power spectrum analysis of monthly SSTAs averaged over the Niño-4 plus Niño-3 region in each experiment (Fig. 6; note that we only show the result longer than 8 years). The SSTAs averaged over this region will largely remove the signal of zonal dipole mode in the DOM (Fig. 5a) and will represent EPDV in all experiments. The result shows that in the SOM, EPDV variance slightly increases longer than 8 year period and then stabilizes after 20 year period (red line in Fig. 6). This relatively stabilized EPDV variance longer than decadal timescales reflects a red spectrum of ocean mixed layers, which can respond to high-frequency atmospheric forcing on low frequencies owing to the large thermal inertia (Frankignoul and Hasselmann 1977; Yu and Boer 2006; Clement et al. 2011; Okumura 2013). EPDV variance in the Clim-τ, in contrast, is significantly lower than that in the SOM (blue line in Fig. 6), indicating the prominent role of mean upwelling in damping equatorial Pacific SSTAs on decadal to multi-decadal timescales.

Compared to the EPDV in the Clim-τ, EPDV is intensified in the DOM (Fig. 2c), suggesting that anomalous wind-driven ocean circulation plays a role in amplifying EPDV. The strength of this amplification, however, is distinct on different timescales (black line in Fig. 6). Specifically, it is strong on decadal (8–20 years) timescales, leading to the EPDV variance in the DOM significantly larger than that in the SOM. In contrast, it becomes insignificantly distinct from that in the SOM on inter-decadal (> 20 years) timescales.

Further, EPDV in the DOM is damped by net surface heat flux (blue contours in Fig. 2c). Together with the dynamical damping by equatorial Pacific mean upwelling revealed from the Clim-τ, EPDV at the mature phase, in the statistical sense (i.e., regression analysis), is generated by anomalous wind-driven ocean circulation, rather than air-sea thermodynamic coupling as seen in the SOM. Note that we do not rule out the possibility that individual EPDV event could arise from thermodynamic coupling.

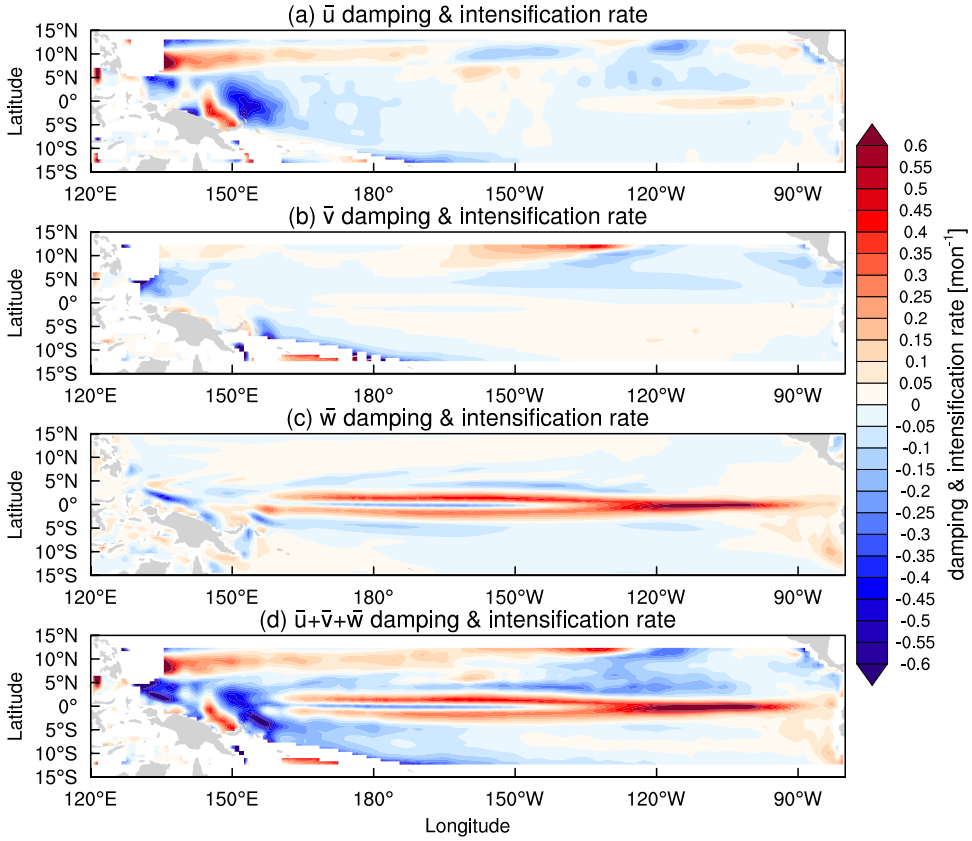

Fig. 4 Estimated EPDV damping and intensification rates in the Clim-τ. **a**–**c** Patterns of the estimated damping (red) and intensification (blue) rates (mon.$^{-1}$) by annual-mean climatological zonal, meridional, and 50 m vertical current, respectively. All the climatological currents are from the Clim-τ experiment. **d** the sum of **a**–**c**

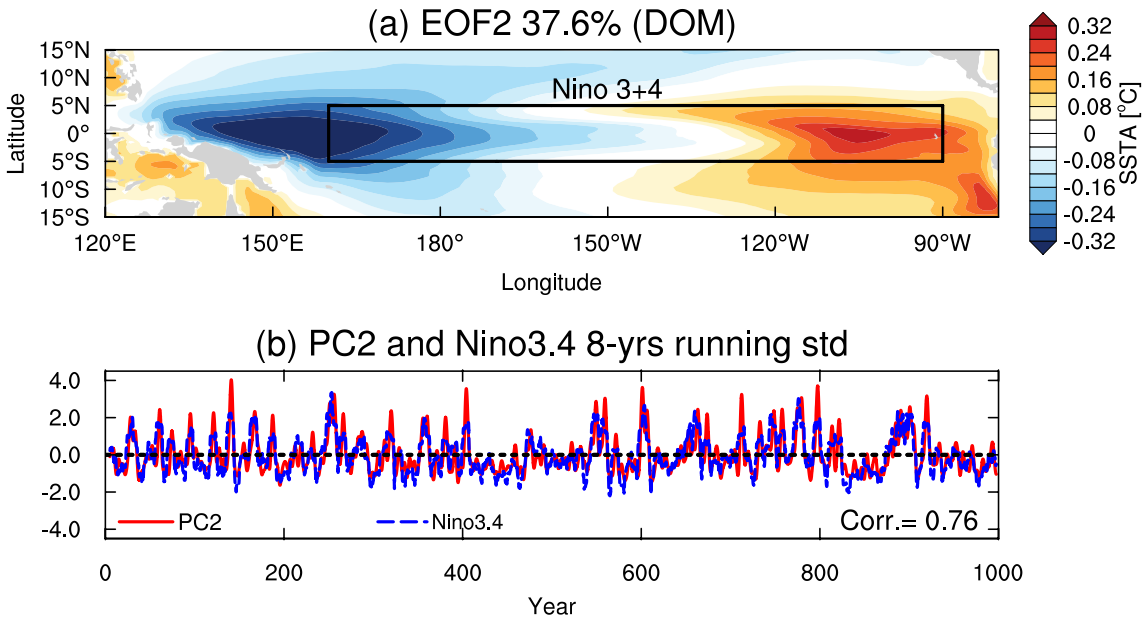

Fig. 5 Zonal dipole mode in the DOM. **a** EOF2 of 8 year low-pass filtered monthly SSTAs in the equatorial Pacific. Black box denotes the Niño-3 plus Niño-4 region (160°E-90°W, 5°S-5°N). **b** The corresponding normalized PC (red line) with normalized 8 year running standard deviation of monthly SSTAs averaged over the Niño-3.4 region (170°W-120°W, 5°S–5°N; blue line). The correlation coefficient between the two time series is labeled in the panel

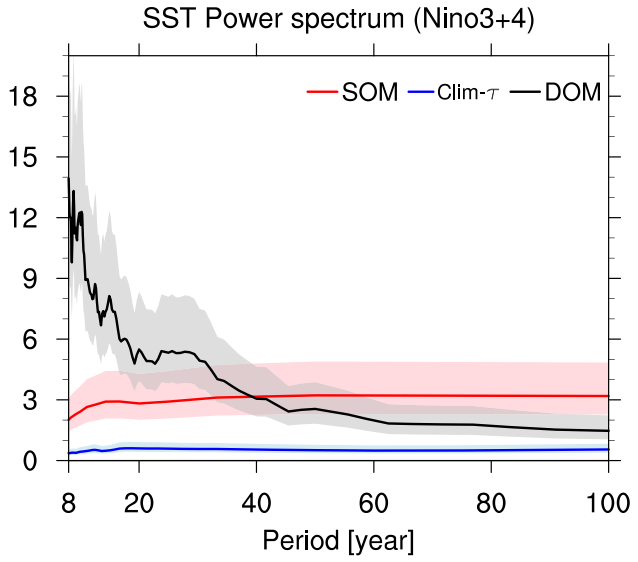

Fig. 6 Power spectra of EPDV in the three experiments. The power spectra (solid lines; °C^2 per (cycles month.$^{-1}$)) are performed based on monthly SSTAs averaged over the black box in Fig. 5a in each experiment. The spectra with periods no less than 8 years are shown. Shading shows the 5–95% confidence interval based on χ^2 statistic. Red: SOM; blue: Clim-τ; black: DOM

To further investigate the role of anomalous wind-driven ocean circulation in EPDV during its temporal evolution, we perform lead-lag regressions of the 8 year low-pass filtered aggregated heat budget terms associated with the effect of anomalous ocean circulation [the third to the last second term on the RHS of Eq. (1)] over the Niño-4 and Niño-3 regions against the normalized EPDV PC in the DOM, respectively (yellow lines in Fig. 7a, b). We also superimpose the lead-lag regressed 8 year low-pass filtered anomalous SST, net heat flux, and upwelling damping term for clarity. The result shows that, first, mean equatorial upwelling is out of phase with EPDV evolution (red vs blue lines in Fig. 7), suggesting that it plays a damping role, a result consistent with the finding in the Clim-τ (Fig. 4). Second, net heat flux anomaly is also basically out of phase with EPDV evolution, suggestive of its damping role (purple lines in Fig. 7). As a consequence, the effect of anomalous ocean circulation must reinforce the damped EPDV and act as a key driver (in phase with EPDV; red vs yellow lines in Fig. 7). Note that the reason that the evolution of the aggregated heat budget terms associated with the effect of anomalous ocean circulation is in phase with EPDV instead of the tendency is that on decadal timescales, the tendency is rather weak, thus resulting in the essentially in-phase evolution with EPDV.

To further examine which key oceanic feedback processes drive EPDV, we perform lead-lag regressions of individual 8 year low-pass filtered heat budget terms associated with the effect of anomalous ocean circulation over the Niño-4 and Niño-3 regions against the normalized EPDV PC in the DOM, respectively (Fig. 8). The result shows that over the Niño-4 region, both zonal advective feedback ($-u'\overline{T}_x$; solid blue line in Fig. 8a) and Ekman pumping feedback ($-w'\frac{\overline{T}_s-\overline{T}_e}{2H}$; solid red line in Fig. 8a) play the dominant driving roles. In contrast, zonal nonlinear heating process ($-u'T'_x$) is negative (dashed blue line in Fig. 8a), representing a stronger damping role for the positive phase of EPDV compared to the negative phase. Specifically, eastward flow

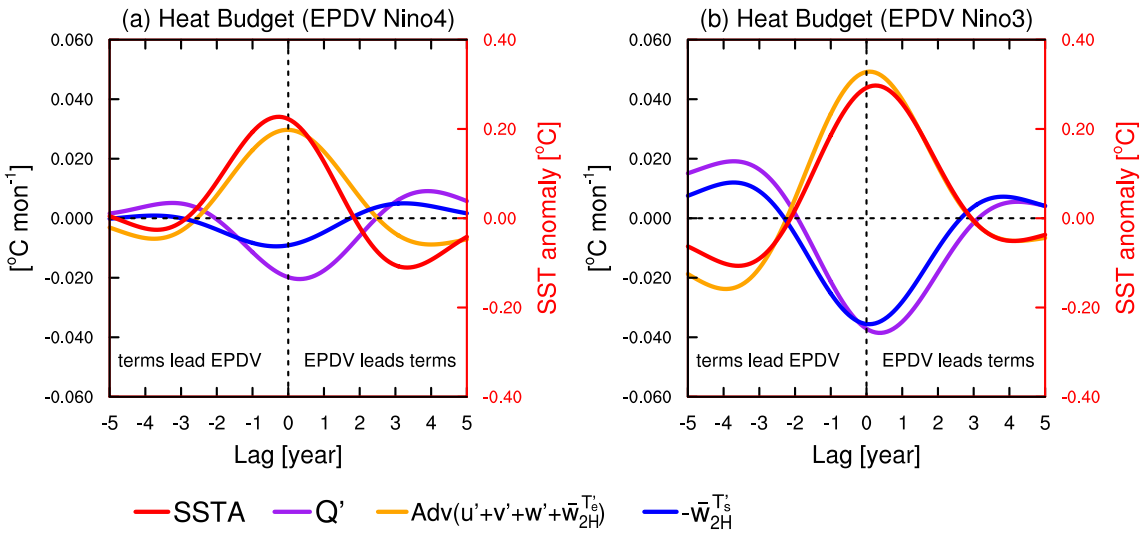

Fig. 7 Lead-lag regressions of 8 year low-pass filtered monthly heat budget terms (°C mon.$^{-1}$) over the (**a**) Niño-4 and (**b**) Niño-3 regions against the normalized EPDV PC in the DOM. Negative (positive) lags represent the tendency terms lead (lag) EPDV. Purple: net surface heat flux; blue: upwelling damping term; yellow: the aggregated term associated with the effect by anomalous ocean circulation. Lead-lag regressed SSTA (red; °C) is superimposed

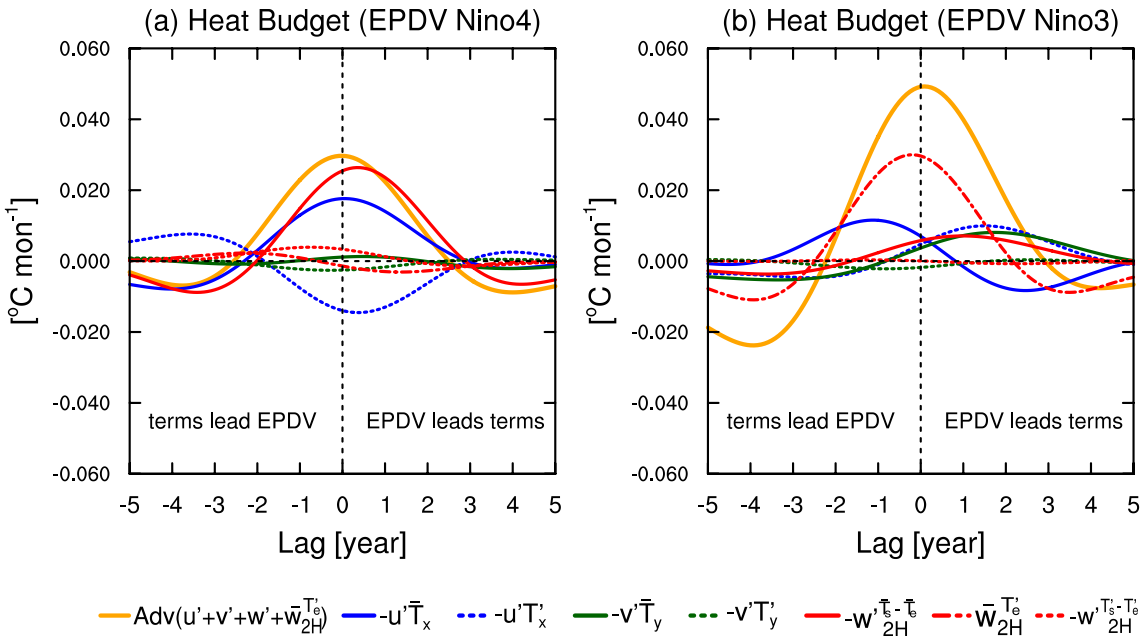

Fig. 8 As in Fig. 7, but for the lead-lag regressed 8 year low-pass filtered individual heat budget terms in the aggregated term associated with the effect by anomalous ocean circulation. Negative (positive) lags represent the tendency terms lead (lag) EPDV. Blue: terms related to anomalous zonal current; green: terms related to anomalous meridional current; red: terms related to anomalous vertical current and subsurface temperature. Yellow lines are the same as those in Fig. 7

anomalies in the central equatorial Pacific driven by westerly anomalies associated with positive EPDV carry the relatively cold temperature anomalies from the west to the central Pacific, therefore damping the positive SSTAs over the Niño-4 region (not shown). Over the Niño-3 region, due to the strong mean upwelljng and thermocline adjustment, thermocline feedback ($\overline{w}\frac{T_e}{2H}$; red dot-dashed line in Fig. 8b) becomes the dominant process in driving EPDV (Fig. 8b). In addition, zonal advective feedback and zonal nonlinear heating process also play the driving and damping roles, respectively, albeit with the phases slightly shifted (Fig. 8b).

4 Origin of EPDV

In the last section, by a step-by-step comparison among the SOM, Clim-τ, and DOM, we have demonstrated that EPDV is primarily driven by ocean–atmosphere dynamic coupling, rather than thermodynamic coupling. In addition to the debate on the driver of EPDV, another controversy is with respect to the origin of EPDV. As reviewed in the introduction, there are two main viewpoints on this controversy: one suggested that EPDV originates from the tropics, such as the interaction with interannual ENSO variability (Chang et al. 2007; Choi et al. 2009, 2012, 2013; Di Lorenzo et al. 2015); the other pointed out that it originates from the extratropics, such as South Pacific variations (Luo and Yamagata 2001; Liguori and Di Lorenzo 2019; Sun and Okumura 2019). In this section, we explore this topic based on the DOM experiment.

To examine the EPDV origin, we perform lead-lag regressions of 8-yr low-pass filtered monthly SST, surface wind, and sea surface height (SSH) anomalies in the tropical Pacific (30°S–30°N) against the normalized EPDV PC in the DOM, from lead of 4 years to lag of 4 years with an 1 year interval (Fig. 9). The results show that at the stage of EPDV development (Fig. 9a–d), there is an SST zonal dipole pattern with slightly warm and cold SSTAs in the western and eastern equatorial Pacific, respectively, at 4- and 3 year leads (Fig. 9a, b). This pattern resembles the negative phase of the zonal dipole mode (ZDM hereafter), the second EOF mode of decadal SST variability in the equatorial Pacific in the DOM (Fig. 5). At 2 year lead, the cold SSTAs in the eastern equatorial Pacific disappear (Fig. 9c) and are subsequently replaced by warm SSTAs at 1 year lead (Fig. 9d). The resultant central-eastern equatorial Pacific warm SSTAs further enhance at 0 year lead (Fig. 9e). At the stage of EPDV decay, the positive SST anomalies first weaken in the central equatorial Pacific (Fig. 9f), and then the pattern of the SSTAs in the equatorial Pacific transforms to the positive phase of the ZDM at 2 year lag (Fig. 9g). After that, the positive SSTAs associated with the ZDM diminish at 3- and 4 year lags (Fig. 9h, i). During the entire EPDV evolution, equatorial Pacific zonal wind and SSH anomalies vary with EPDV,

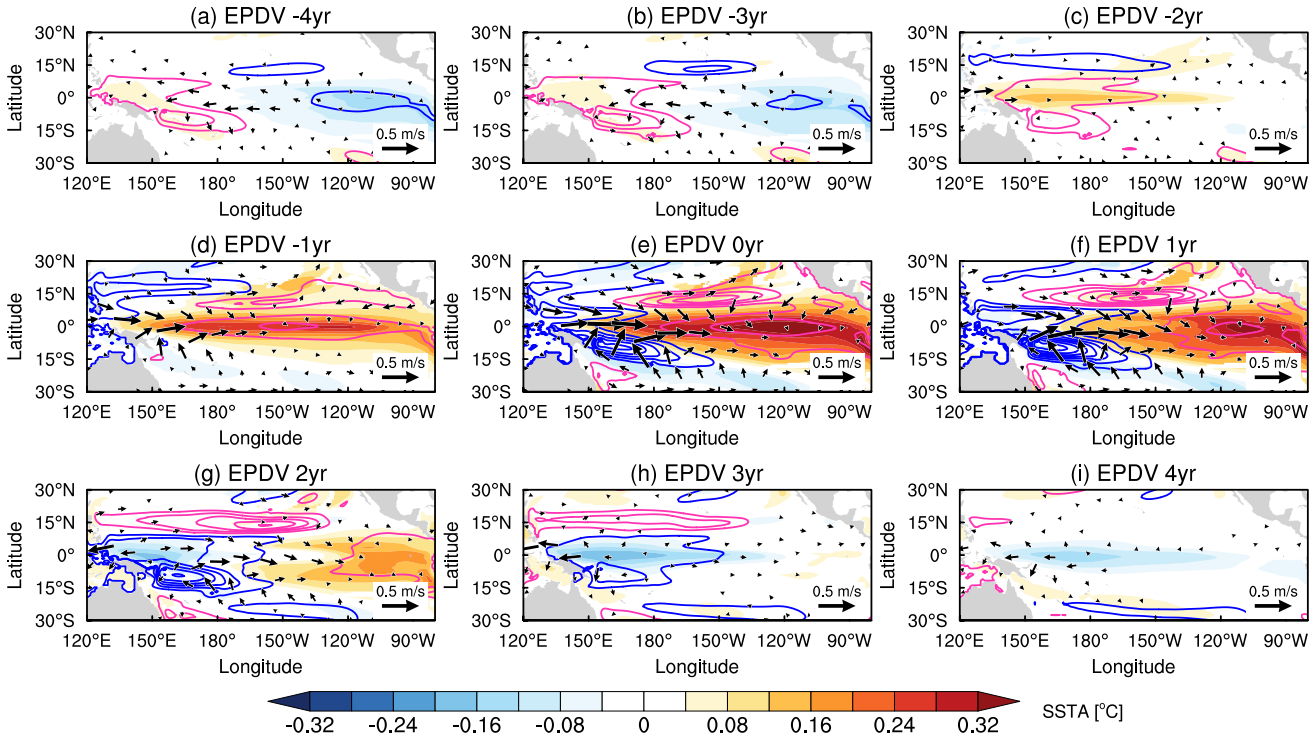

Fig. 9 Lead-lag regressions of 8 year low-pass filtered monthly SST (shading; °C), surface wind (vectors; m s.$^{-1}$), and SSH (contour interval: 0.5 cm; purple is positive and blue is negative) anomalies against the normalized EPDV PC in the DOM. The regressions significant at the 95% confidence level based on a two-tailed Student's *t*-test are shown only, except for the regressed SSH, which is shown as a whole for clarity

suggesting a dynamically coupled ocean–atmosphere variability in the equatorial Pacific.

The above presented results imply a possible transition process between EPDV and the ZDM with ~ 2 year interval. To further verify their relationship, we perform lead-lag correlation between their PC time series. The result shows that EPDV and the ZDM are significantly (at the 95% confidence level) correlated with each other at approximately 2 year lead and lag (Fig. 10), indicative of their transition process.

During the evolution of EPDV, in addition to the variations in the equatorial Pacific, some variations in the extra-equatorial Pacific are worth noting. In particular, before the mature phase of EPDV (Fig. 9a–d), negative SSH anomalies in the central North Pacific (along 15°N) emerge at 4- and 3 year leads (Fig. 9a, b). Subsequently, they propagate westward and ultimately arrive at the western boundary at 0 year lead (Fig. 9c–e). After the mature phase of EPDV (Fig. 9f–i), the previous negative SSH anomalies at 15°N are replaced by positive anomalies, which are strengthened and propagate westward. These characteristics of the evolution of the SSH anomalies indicate the westward-propagating oceanic Rossby waves, which may transform to equatorially trapped oceanic Kelvin waves that propagate eastward to impact the phase transition of EPDV. This extra-equatorial Pacific Rossby adjustment for EPDV was documented in the EPDV literature (Meehl and Hu 2006; Power et al. 2021). The above analyses further demonstrate that in the DOM, EPDV originates from ocean–atmosphere dynamic coupling in the tropical Pacific.

5 Summary and discussion

While it is known that ocean dynamics plays an essential role in EPDV, its role is obscured by SOM in simulating the air-sea thermodynamically coupled EPDV. To confront this issue, we took advantage of the Clim-τ, which removes the effect of anomalous wind-driven ocean circulation on EPDV by imposing climatological wind stress over the tropical Pacific. This experiment, therefore, bridges the dynamical framework between SOM and DOM. By comparing SOM to the Clim-τ, we explored the role of mean ocean circulation and showed that mean equatorial Pacific upwelling plays a key role in damping EPDV. By comparing the Clim-τ to DOM, we investigated the role of anomalous wind-driven ocean circulation and demonstrated that it plays a role in amplifying the damped EPDV. The strength of the amplification, in fact, overwhelms the damping effect by mean upwelling, resulting in the anomalous wind-driven ocean circulation

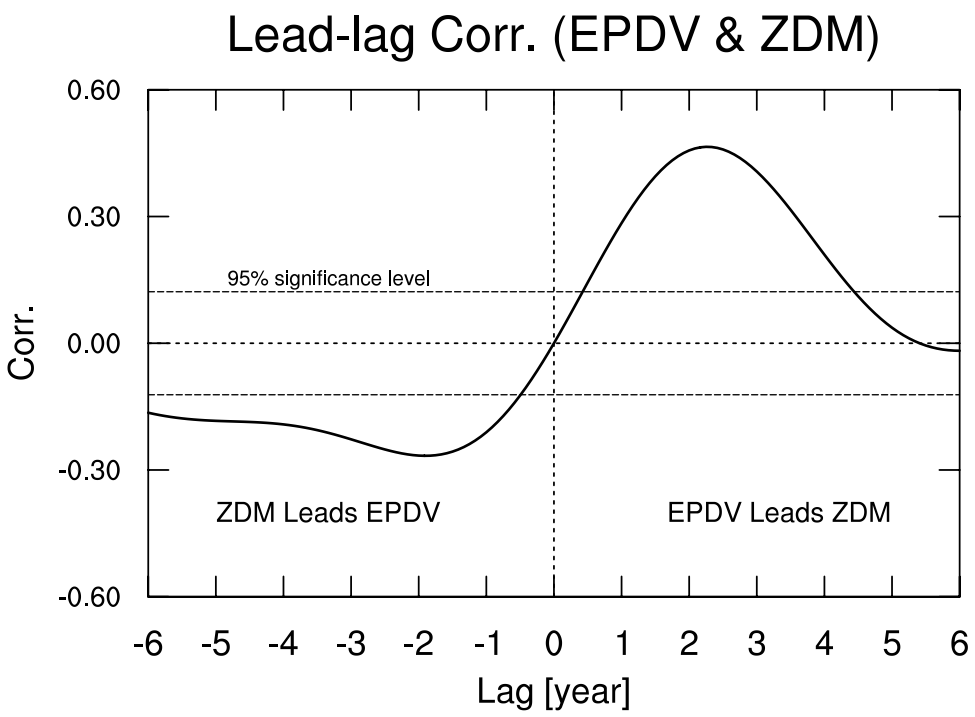

Fig. 10 Lead-lag correlations between the PC of EPDV and the ZDM in the DOM. Dashed horizontal lines represent the correlations significant at the 95% confidence level based on a two-tailed Student's *t* test

becoming the driver of EPDV. This is the case for the entire evolution of EPDV. Taking EPDV as an example, our study advances the understanding of the two distinct dynamical systems (i.e., SOM and DOM), shedding light on interpreting the role of ocean dynamics in other climate variabilities and ocean basins.

Aside from unravelling the role of ocean dynamics in EPDV, we also explored the origin of EPDV. Our analyses suggested that in the CM2.1 DOM, EPDV originates primarily from tropical Pacific decadal variability, which is related to the ZDM (Figs. 9 and 10). Specifically, the positive phase of EPDV can develop from the negative phase of the ZDM about 2 years ago, and can transform to the positive phase of the ZDM after ~ 2 years. As a result, EPDV and the ZDM are interplayed with each other. Although our study provides a new insight for the EPDV origin, this issue is still outstanding (i.e., tropical vs extratropical origin; Luo and Yamagata 2001; Sun and Okumura 2019; Power et al. 2021). The proposed hypothesis on the EPDV-ZDM interaction is worth further investigating based on observations and DOMs from other climate models.

Acknowledgements We appreciate three anonymous reviewers for providing constructive comments and substantially improving the manuscript.

Funding Y.Z. and X.L. were supported by the National Natural Science Foundation of China (92058203 and 41925025). Y.Z. was supported by the Fundamental Research Funds for the Central Universities (202213050) and the project funded by China Postdoctoral Science Foundation (2021M703034). Q.P. was supported by the National Natural Science Foundation of China (42005035) and the Science and Technology Planning Project of Guangzhou (202102020935). Y.K. was supported by the Japan Society for the Promotion of Science (JP18H01278 and JP19H05703) and the Japanese Ministry of Education, Culture, Sports, Science and Technology (JPMXD0717935457 and JPMXD1420318865). J.-C.Y. was supported by the National Natural Science Foundation of China (42105019 and 92058203) and the project funded by China Postdoctoral Science Foundation (2020M672138). S.M.L. was supported by the National Science Foundation (AGS-1951713). A.J.M. was supported by the National Science Foundation (OCE2022868 and CCE-LTER OCE1637632) and NOAA (MAPP NA17OAR4310106). L.F. was supported by the Natural Science Foundation of China (41975089).

Data availability The SOM data are available from: https://nomads.gfdl.noaa.gov/dods-data/gfdl_sm2_1/MLM2.1U_Control-1990_D1/pp/atmos/ts/monthly/. The Clim-τ data are available from: https://data.mendeley.com/datasets/ctn5k77ttr/draft?a=c9db68b4-d4af-48a4-b14d-709edc7fa1b7. The DOM data are available from: https://data.mendeley.com/datasets/mrg8g4w9zk/draft?a=4d2e535f-7dc6-4f10-b2ad-c1bf565637ce

Declarations

Conflict of interest The authors declare that there are no conflicts of interest or competing interests regarding the publication of this paper.

References

An SI (2009) A review of interdecadal changes in the nonlinearity of the El Niño-Southern oscillation. Theor Appl Climatol 97:29–40. https://doi.org/10.1007/s00704-008-0071-z

Barnett TP, Pierce DW, Latif M, Dommenget D, Saravanan R (1999) Interdecadal interactions between the tropics and midlatitudes in the Pacific basin. Geophys Res Lett 26:615–618. https://doi.org/10.1029/1999GL900042

Capotondi A (2013) ENSO diversity in the NCAR CCSM4 climate model. J Geophys Res Oceans 118:4755–4770. https://doi.org/10.1002/jgrc.20335

Capotondi A, Alexander MA (2001) Rossby waves in the tropical North Pacific and their role in decadal thermocline variability. J Phys Oceanogr 31:3496–3515. https://doi.org/10.1175/1520-0485(2002)031%3c3496:RWITTN%3e2.0.CO;2

Capotondi A, Alexander MA, Deser C, McPhaden MJ (2005) Anatomy and decadal evolution of the Pacific subtropical–tropical cells (STCs). J Clim 18:3739–3758. https://doi.org/10.1175/JCLI3496.1

Chang P, Zhang L, Saravanan R et al (2007) Pacific meridional mode and El Niño-Southern oscillation. Geophys Res Lett. https://doi.org/10.1029/2007GL030302

Choi J, An SI, Dewitte B, Hsieh WW (2009) Interactive feedback between the tropical Pacific decadal oscillation and ENSO in a coupled general circulation model. J Clim 22:6597–6611. https://doi.org/10.1175/2009JCLI2782.1

Choi J, An SI, Yeh SW (2012) Decadal amplitude modulation of two types of ENSO and its relationship with the mean state. Clim Dyn 38:2631–2644. https://doi.org/10.1007/s00382-011-1186-y

Choi J, An SI, Yeh SW, Yu JY (2013) ENSO-like and ENSO-induced tropical Pacific decadal variability in CGCMs. J Clim 26:1485–1501. https://doi.org/10.1175/JCLI-D-12-00118.1

Clement A, Di Nezio P, Deser C (2011) Rethinking the ocean's role in the Southern Oscillation. J Clim 24:4056–4072. https://doi.org/10.1175/2011JCLI3973.1

Cobb KM, Charles CD, Cheng H, Edwards RL (2003) El Niño/Southern Oscillation and tropical Pacific climate during the last millennium. Nature 424:271–276. https://doi.org/10.1038/nature01779

Delworth TL, Broccoli AJ, Rosati A et al (2006) GFDL's CM2 global coupled climate models. Part I: formulation and simulation characteristics. J Clim 13:643–674. https://doi.org/10.1175/JCLI3629.1

Di Lorenzo E, Liguori G, Schneider N, Furtado JC, Anderson BT, Alexander MA (2015) ENSO and meridional modes: a null hypothesis for Pacific climate variability. Geophys Res Lett 42:9440–9448. https://doi.org/10.1002/2015GL066281

DiNezio PN, Kirtman BP, Clement AC, Lee SK, Vecchi GA, Wittenberg A (2012) Mean climate controls on the simulated response of ENSO to increasing greenhouse gases. J Clim 25:7399–7420. https://doi.org/10.1175/JCLI-D-11-00494.1

Dommenget D, Latif M (2008) Generation of hyper climate modes. Geophys Res Lett. https://doi.org/10.1029/2007GL031087

Frankignoul C, Hasselmann K (1977) Stochastic climate models. Part II: application to sea-surface temperature anomalies and thermocline variability. Tellus 29A:289–305. https://doi.org/10.3402/tellusa.v29i4.11362

Graffino G, Farneti R, Kucharski F, Molteni F (2019) The effect of wind stress anomalies and location in driving Pacific subtropical cells and tropical climate. J Clim 32:1641–1660. https://doi.org/10.1175/JCLI-D-18-0071.1

Hua L, Yu Y, Sun DZ (2015) A further study of ENSO rectification: results from an OGCM with a seasonal cycle. J Clim 28:1362–1382. https://doi.org/10.1175/JCLI-D-14-00404.1

Jin F-F, Kim ST, Bejarano L (2006) A coupled-stability index for ENSO. Geophys Res Lett. https://doi.org/10.1029/2006GL027221

Kim GI, Kug JS (2020) Tropical Pacific decadal variability induced by nonlinear rectification of El Niño-Southern Oscillation. J Clim 33:7289–7302. https://doi.org/10.1175/JCLI-D-19-0123.1

Kim SB, Lee T, Fukumori I (2007) Mechanisms controlling the interannual variation of mixed layer temperature averaged over the Niño-3 region. J Clim 20:3822–3843. https://doi.org/10.1175/JCLI4206.1

Larson SM, Kirtman BP (2015) Revisiting ENSO coupled instability theory and SST error growth in a fully coupled model. J Clim 28:4724–4742. https://doi.org/10.1175/JCLI-D-14-00731.1

Larson SM, Vimont DJ, Clement A, Kirtman BP (2018a) How momentum coupling affects SST variance and large-scale Pacific climate variability in CESM. J Clim 31:2927–2944. https://doi.org/10.1175/JCLI-D-17-0645.1

Larson SM, Pegion KV, Kirtman BP (2018b) The South Pacific meridional mode as a thermally driven source of ENSO amplitude modulation and uncertainty. J Clim 31:5127–5145. https://doi.org/10.1175/JCLI-D-17-0722.1

Li J, Xie S-P, Cook ER et al (2011) Interdecadal modulation of El Niño amplitude during the past millennium. Nat Clim Chang 1:114–118. https://doi.org/10.1038/nclimate1086

Liguori G, Di Lorenzo E (2019) Separating the North and South Pacific meridional modes contributions to ENSO and tropical decadal variability. Geophys Res Lett 46:906–915. https://doi.org/10.1029/2018GL080320

Liu C, Zhang W, Stuecker MF, Jin F-F (2019) Pacific Meridional Mode-Western North Pacific tropical cyclone linkage explained by tropical Pacific quasi-decadal variability. Geophys Res Lett 46:13346–13354. https://doi.org/10.1029/2019GL085340

Luo J-J, Yamagata T (2001) Long-term El Niño-Southern Oscillation (ENSO)-like variation with special emphasis on the South Pacific. J Geophys Res Oceans 106:22211–22227. https://doi.org/10.1029/2000JC000471

McPhaden MJ, Zhang D (2002) Slowdown of the meridional overturning circulation in the upper Pacific Ocean. Nature 415:603–608. https://doi.org/10.1038/415603a

Meehl GA, Hu A (2006) Megadroughts in the Indian monsoon region and southwest North America and a mechanism for associated multidecadal Pacific sea surface temperature anomalies. J Clim 19:1605–1623. https://doi.org/10.1175/JCLI3675.1

Ogata T, Xie S-P, Wittenberg A, Sun DZ (2013) Interdecadal amplitude modulation of El Niño-Southern Oscillation and its impact on tropical Pacific decadal variability. J Clim 26:7280–7297. https://doi.org/10.1175/JCLI-D-12-00415.1

Okumura YM (2013) Origins of tropical Pacific decadal variability: role of stochastic atmospheric forcing from the South Pacific. J Clim 26:9791–9796. https://doi.org/10.1175/JCLI-D-13-00448.1

Pierce DW, Barnett TP, Latif M (2000) Connections between the Pacific Ocean tropics and midlatitudes on decadal timescales. J Clim 13:1173–1194. https://doi.org/10.1175/1520-0442(2000)013%3c1173:CBTPOT%3e2.0.CO;2

Power S, Colman R (2006) Multi-year predictability in a coupled general circulation model. Clim Dyn 26:247–272. https://doi.org/10.1007/s00382-005-0055-y

Power S, Lengaigne M, Capotondi A et al (2021) Decadal climate variability in the tropical Pacific: characteristics, causes, predictability, and prospects. Science 374:eaay9165. https://doi.org/10.1126/science.aay9165

Rodgers KB, Friederichs P, Latif M (2004) Tropical Pacific decadal variability and its relation to decadal modulations of ENSO. J Clim 17:3761–3774. https://doi.org/10.1175/1520-0442(2004)017%3c3761:TPDVAI%3e2.0.CO;2

Santoso A, McPhaden MJ, Cai W (2017) The defining characteristics of ENSO extremes and the strong 2015/2016 El Niño. Rev Geophys 55:1079–1129. https://doi.org/10.1002/2017RG000560

Stouffer RJ, Broccoli AJ, Delworth TL et al (2006) GFDL's CM2 global coupled climate models. Part IV: idealized climate response. J Clim 19:723–740. https://doi.org/10.1175/JCLI3632.1

Sun T, Okumura YM (2019) Role of stochastic atmospheric forcing from the South and North Pacific in tropical Pacific

decadal variability. J Clim 32:4013–4038. https://doi.org/10.1175/JCLI-D-18-0536.1

Sun F, Yu J-Y (2009) A 10–15-yr modulation cycle of ENSO intensity. J Clim 22:1718–1735. https://doi.org/10.1175/2008JCLI2285.1

Sun DZ, Zhang T, Sun Y, Yu Y (2014) Rectification of El Niño-Southern Oscillation into climate anomalies of decadal and longer time scales: results from forced ocean GCM experiments. J Clim 27:2545–2561. https://doi.org/10.1175/JCLI-D-13-00390.1

Tatebe H, Imada Y, Mori M, Kimoto M, Hasumi H (2013) Control of decadal and bidecadal climate variability in the tropical Pacific by the off-equatorial South Pacific Ocean. J Clim 26:6524–6534. https://doi.org/10.1175/JCLI-D-12-00137.1

Timmermann A (2003) Decadal ENSO amplitude modulations: a nonlinear paradigm. Global Planet Change 37:135–156. https://doi.org/10.1016/S0921-8181(02)00194-7

Timmermann A et al (2018) El Niño-Southern oscillation complexity. Nature 559:535–545. https://doi.org/10.1038/s41586-018-0252-6

Vimont D (2005) The contribution of the interannual ENSO cycle to the spatial pattern of decadal ENSO-like variability. J Clim 18:2080–2092. https://doi.org/10.1175/JCLI3365.1

Watanabe M, Wittenberg AT (2012) A method for disentangling El Niño–mean state interaction. Geophys Res Lett. https://doi.org/10.1029/2012GL052013

Xie S-P, Philander SGH (1994) A coupled ocean-atmosphere model of relevance to the ITCZ in the eastern Pacific. Tellus 46A:340–350. https://doi.org/10.3402/tellusa.v46i4.15484

Yang J-C, Zhang Y, Lin X, Chang P (2021) Optimal growth of IPV lags AMV modulations by up to a decade. Geophys Res Lett 48:e2021GL096654. https://doi.org/10.1029/2021GL096654

Yeh S-W, Kirtman BP (2004) Tropical Pacific decadal variability and ENSO amplitude modulation in a CGCM. J Geophys Res Oceans. https://doi.org/10.1029/2004JC002442

Yu B, Boer GJ (2006) The variance of sea surface temperature and projected changes with global warming. Clim Dyn 26:801–821. https://doi.org/10.1007/s00382-006-0117-9

Zhang Y, Wallace JM, Battisti DS (1997) ENSO-like interdecadal variability: 1900–1993. J Clim 10:1004–1020. https://doi.org/10.1175/1520-0442(1997)010%3c1004:ELIV%3e2.0.CO;2

Zhang H, Clement A, Di Nezio P (2014a) The South Pacific meridional mode: a mechanism for ENSO-like variability. J Clim 27:769–783. https://doi.org/10.1175/JCLI-D-13-00082.1

Zhang H, Deser C, Clement A, Tomas R (2014b) Equatorial signatures of the Pacific Meridional Modes: dependence on mean climate state. Geophys Res Lett 41:568–574. https://doi.org/10.1002/2013GL058842

Zhang Y, Yu S, Amaya DJ et al (2021) Pacific meridional modes without equatorial Pacific influence. J Clim 34:5285–5301. https://doi.org/10.1175/JCLI-D-20-0573.1

Zhao Y, Di Lorenzo E (2020) The impacts of extra-tropical ENSO precursors on tropical Pacific decadal-scale variability. Sci Rep 10:3031. https://doi.org/10.1038/s41598-020-59253-3